Physical Review Materials 5, 083607 (2021)

10.1103/PhysRevMaterials.5.083607

Bifurcation of nanoscale thermolubric friction behavior for sliding on MoS₂

Kathryn R. Hasz, ¹ Mohammad R. Vazirisereshk, ² Ashlie Martini, ² Robert W. Carpick^{1,3}

- Department of Materials Science and Engineering, University of Pennsylvania,
 Philadelphia, Pennsylvania 19104, United States
- Department of Mechanical Engineering, University of California, Merced, California
 95343, United States
- Department of Mechanical Engineering and Applied Mechanics, University of Pennsylvania, Philadelphia, Pennsylvania 19104, United States

ABSTRACT

We present atomic force microscopy (AFM) experiments of wearless sliding between nanoscale tips and both bulk and monolayer MoS₂ in ultrahigh vacuum across a wide range of temperatures and scanning speeds. Atomic lattice stick-slip behavior is consistently resolved. However, a bifurcation of behavior is seen, with some measurements showing a strong decrease in friction with increasing temperature and others showing athermal and low friction under nominally identical conditions. The difference between thermal and athermal behavior is attributed to a change in the corrugation of the potential energy surface, potentially due to

trace amounts of adsorbed contaminants. While the speed dependence at a given temperature is consistent with the thermal Prandtl-Tomlinson model for atomic-scale friction, that is not the case for the temperature dependence (when it is present), nor can the temperature dependence be described by other existing models. We discuss the limitations of these models in light of the measured results.

INTRODUCTION

Layered materials such as graphite and MoS₂ have been used as solid lubricants for decades in applications from cutting tools to spacecraft bearings, due in large part to the low interfacial shear forces between their weakly-bonded layers¹. More recently, their 2D analogues, monolayer or few-layer graphene and MoS₂, have garnered extensive interest due to their extreme physical properties. These 2D materials also offer low friction, and are currently being explored as additives for commercial lubricants^{2–4} and as ultrathin protective coatings.^{5,6} Such applications require reliable function over a wide range of operating conditions, including sliding speeds and temperatures. While there has been extensive investigation into the macroscale behavior of dry sliding contacts,^{7–9} the fundamental mechanisms behind the low friction behavior of these contacts, and the factors which limit it, remain unclear.¹⁰

There have been numerous prior investigations into the influence of sliding speed and temperature on nanoscale friction, particularly in the wearless regime^{11–14}. Frequently, the results of these studies are analyzed using the thermal Prandtl-Tomlinson (PTT) model. The PTT model is a reduced order model in which a point mass is pulled through a periodically corrugated potential energy surface via an elastic spring. The corrugation of the periodic potential causes

resistance to sliding. Thermal fluctuations provide additional energy to the point mass, allowing it to overcome energy barriers sooner than it would without thermal energy. Mathematically, the static friction of sliding in the PTT model can be calculated by 15–19

$$\frac{1}{\beta k_B T} (F_C - F_F)^{3/2} = \ln \frac{v_0}{v} - \frac{1}{2} \ln \left(1 - \frac{F_F}{F_C} \right), \tag{1}$$

where θ is a parameter describing the shape of the periodic potential, T is the temperature, F_c is the friction force at 0 K, v is the sliding speed, and F_F is the measured static friction. The so-called critical velocity term is $v_0 = \frac{2f_0\beta k_BT}{3k\sqrt{F_c}}$, with f_0 being an attempt frequency and k being the lateral spring constant of the tip-sample system. For the case of sinusoidal potential of periodicity (lattice spacing) a and amplitude U, $\beta_{sin} = \frac{3\pi\sqrt{F_c}}{2\sqrt{2}a}$ and $F_c = \frac{\pi U}{a}$.

The transcendental equation assumes that the system resides into a "thermal activation" regime where $k_BT << U$. Thus, slips are infrequent, and backward jumps do not occur. In this case, temperature and speed play considerable roles. Equation (1) can be further simplified for the case where v/v_0 approaches but does not exceed 1, producing the equation:¹⁵

$$F_F = F_C - \left| \beta k_B T \ln \frac{v_0}{v} \right|^{2/3}, \tag{2}$$

These relations predict a decrease in friction with increasing temperature that has been seen experimentally, an effect termed "thermolubricity" 20,21.

If $v << v_0$ and/or $k_B T >> U$, the system is described as being in the "thermal drift" regime, in which thermal hopping from one energy well to the next occurs, whereby:²²

$$F_F = C^* \frac{U}{k_B T} exp\left(\frac{U}{k_B T}\right) \eta M v. \tag{3}$$

In this case M is the effective mass, C^* is a dimensionless factor related to the width of the energy barrier, and η is a damping parameter. Small changes in temperature or scanning speed have a

reduced influence in comparison with the thermal activation regime, but friction overall is low.

In this regime, friction again decreases with increasing temperature.

The PTT model represents, in a simplified way, the setup of an atomic force microscopy (AFM) experiment, in which a cantilever with a small tip having a radius typically on the order of tens of nanometers is pulled across a periodic crystal surface. Many AFM experiments have reported a nearly-logarithmic increase in friction with increasing sliding speed, consistent with the behavior predicted by the PTT model in the thermal activation regime, for material pairs including Si on mica, 16 Si on gold, 14 Si on NaCl and highly ordered pyrolytic graphite (HOPG), 12,23,24 Si on HOPG, 25 Si on bulk and monolayer MoS₂, 26,27 among others. Acikgoz et al. have extended the work on the speed dependence of friction for the case of a Si tip sliding on exfoliated monolayer and bulk MoS₂.²⁶ They found that both monolayer and bulk MoS₂ showed a logarithmic increase in friction force with sliding speed, consistent with the PTT model. However, they observed evolution of the magnitude of the friction force over multiple scan sets, which they attributed to evolution of the tip with prolonged scanning. Molecular dynamics (MD) simulations of a similar setup also showed this nearly-logarithmic dependence, e.g. ^{13,14}. For example, Li et al. used AFM experiments and MD simulations to study a Pt tip sliding on an Au(111) surface¹³. While both the experimental and simulated friction trends agreed well with the PTT model, there was a difference in speed between experiments and simulations. The speed range was later extended by Liu, et al. to reach overlapping speeds between AFM experiments and MD simulations of a Si tip sliding on a Au(111) surface¹⁴. This speed dependence was fit to the transcendental form of the PTT equation. By correcting for tip area and mass differences, the experimental and simulation data agreed with each other.

There has also been work on the temperature-dependent friction force predictions of the PTT model. Zhao et al. observed a dramatic increase in friction force with decreasing temperature for silicon nitride tips sliding on HOPG, MoS₂ and PbS crystalline samples^{28–30} measured in ultrahigh vacuum (UHV) from 750K down to 100K. Below approximately 200K, the behavior became athermal, which was attributed to wear. They used an Arrhenius model to describe the thermallydependent data, obtaining good fits. This indicated that, provided there was no wear, friction exhibited thermally-activated behavior. Comparison to the PTT model was not made, and sliding speed was not varied. Recent work by Liu, et al.³¹ used a similar Arrhenius model to describe the temperature dependence of a graphite-wrapped tip sliding on graphite. They also observed an approximately logarithmic increase in friction with increasing scanning speed at room temperature. However, no speed dependence was studied at different temperatures nor were the results compared to the PTT model. Perez et al. used a rate theory based model to describe atomic scale friction behavior over a wide range of temperatures and velocities. 32 The predicted friction trend was in agreement with the 1D PTT model. Steiner et al. used a modified 2D PTT numerical simulation to investigate friction on NaCl and HOPG and see a decrease in friction with increasing temperature, with the effect more pronounced with higher energy barriers to sliding.33 Sills et al. found an approximately logarithmic increase in friction force with increasing speed and decrease with increasing temperature, although their system was a glassy polystyrene surface which does not have a well-defined periodic potential³⁴; however, the existence of multiple local energy minima in the tip-sample potential energy surface could lead to PTT-like behavior. Jansen et al. were able to produce a good fit to the PTT model for friction data measured using Si tips sliding on HOPG in UHV from 100-300 K and over a range of sliding speeds. The best fits were

obtained when the attempt frequency f_0 was allowed to vary freely (variations between 5 and 120 MHz, with no uniform trend with temperature, led to the best fit). Schirmeisen and coworkers observed a non-monotonic trend of friction force increasing as temperature decreased from room temperature in UHV for silicon tips sliding on Si with its native oxide. Friction increased until approximately 100 K, at which temperature friction began to decrease again as the temperature was further lowered. This non-monotonic trend was explained using a multibond (MB) model, which fit the data well. 11,12,23,24 The MB model assumes multiple local "bonds" at the tip sample interface that have different barriers both for forming and breaking, the latter being greater than the former. This leads to a thermally activated increase, and then decrease, in friction.

In this work, we investigate the temperature and speed dependence of friction for tips (using three different tip materials) sliding on bulk and monolayer MoS₂ in UHV, from cryogenic to elevated temperatures. We observe two distinct characteristic sets of behaviors: in some cases, pronounced thermolubricity occurs where friction decreases with increasing temperature, while in other cases, almost no temperature dependence is seen and friction is low. By obtaining data with tests performed at a dense array of speed/temperature combinations, we are able to thoroughly probe the applicability of the PTT model. While the PTT model captures the speed dependence reasonably well for most of the measurements, it does not describe the temperature dependence. Through the use of a previously developed numerical model³⁵ based on a 2D PTT approach, insights into the effects of energy barrier and lateral stiffness on atomic scale friction are gained.

II. METHODS

All friction measurements were obtained with an RHK 750 AFM (RHK Tech, Troy, Michigan) under ultrahigh vacuum (UHV) conditions with pressure less than 8e-10 torr, unless stated otherwise. Measurements were performed on the basal plane of bulk MoS₂ (SPI Supplies, West Chester, PA) and on monolayer MoS₂ grown by chemical vapor deposition (CVD) using the method of Naylor et al.³⁶, provided by the group of A.T. Johnson, University of Pennsylvania. Both the bulk form and a CVD-grown monolayer of MoS₂ were used to assess the effect of sample preparation technique and sample thickness on friction-temperature dependence. The bulk MoS₂ was transferred into the UHV chamber within 30 minutes of mechanical exfoliation, and the CVD sample was transferred into the chamber within 1 hour of growth. Both samples were then annealed at 150 °C for at least 2 hours under vacuum to desorb contaminants. Commercial contact-mode cantilevers with integrated tips of Si₃N₄ (MikroMasch, Watsonville, CA), Si with native oxide (MikroMasch, Watsonville, CA), and ultrananocrystalline diamond (UNCD) (ADT, Romeoville, IL) were used for measurements. The normal spring constants ranged from 0.05-1.5 N/m depending on the cantilever geometry and material and were calibrated using the thermal tune method.³⁷ Lateral forces were calibrated using the diamagnetic lateral force calibration method³⁸, with lateral force spring constants ranging from 0.05-5 N/m.

The sample temperature was controlled using a LN_2 flow cryostat for cooling and a tungsten resistive heater mounted in the sample holder for heating, with both used simultaneously at times to access a temperature range of 140-500 K. Temperature was measured using a K-type thermocouple attached to the top sample surface. The system was left to stabilize until the temperature changed less than 10 K per hour. All reported temperatures are accurate to ± 2 K.

Temperature was varied sequentially by increasing temperature from room temperature to elevated temperatures, then reducing back to room temperature, then further reducing to cryogenic temperatures, and finally increasing back to room temperature. No hysteresis effects were seen between data obtained as temperature was increasing from 140 K to 500 K nor as temperature was decreasing from 500 K to 140 K.

Scan speeds ranging over 5 decades, from 5 nm/s to 500 μ m/s, were used with two different measurement techniques. Full 2D friction images were obtained at speeds of 17, 33, and 66 nm/s with 256 lines/image and friction averaged from all lines. Individual line scans of a single 100 nm loop were obtained for the whole speed range, with friction obtained by averaging over 8 friction loops. Friction force values were determined by measuring half of the average value of the difference between peak heights in the forward and backward scans, as is standard for measuring static friction. All measurements were taken at zero applied load, with the load regularly monitored with force-distance curves and adjustments of the zero point as needed. A full set of these measurements was performed at each temperature. No signs of sample inhomogeneity were observed in the friction or topography images. From topographic images, the root-mean-squared roughness over 100 x 100 nm² areas was measured to be 0.43 \pm 0.01 nm for the bulk MoS2, and 0.42 \pm 0.02 nm for the CVD MoS2 sample.

Pull-off force measurements were performed at the beginning, middle, and end of measurement sets at each temperature. While in many cases the adhesion forces for a given tip were consistent as the temperature was varied, some sets had widely ranging pull off forces that varied by at least a factor of 3 between subsequent measurements in a single dataset (i.e. between pull off forces taken at one temperature and pull off forces taken at the next

temperature). Accordingly, datasets were processed both with all data included, and by selecting only subsets of data that had an approximately constant pull-off force, i.e., with a change of less than 20% for sequential temperatures. No net temperature dependence was seen in the adhesion force, consistent with other recent AFM studies. 11,12,31

Complementary MD simulations were designed to match the AFM experiment as closely as possible. In these simulations, an amorphous silicon nitride tip (details on the amorphization process in section S1) was slid over a MoS_2 substrate. To further match the simulation and experiments, the MD tip apex shape was designed based on the transmission electron microscopy (TEM) image of one of the experimental silicon nitride AFM tip apices. We traced the tip apex in a high-resolution TEM image of the tip to extract the 2D profile of the tip apex and measured a tip radius of 25 ± 5 nm. We then used the method of disks³⁹ to create the 3D tip from the 2D profile assuming that the 2D profile is representative of the tip shape in all orientations^{40,41}.

The interactions of the atoms within the substrate and the within the tip were described using the REBO 42 and the Tersoff potential 43 respectively. The Lennard Jones interaction parameters between tip and substrate were tuned so that the adhesion force obtained from MD simulation, 12.8 nN, was consistent with the corresponding experimental adhesion value of 12.1 \pm 0.3 nN obtained with the matching tip. The tip was coupled to an interaction-free particle acting as the AFM cantilever, which moves with constant speed, using a spring with 1.6 N/m stiffness to take into account the lateral compliance of the AFM cantilever. The lateral force microscopy simulation was performed by translating the interaction-free particle with speeds of 1 m/s and 3 m/s at temperature ranging from 200-470 K with no applied normal load. The bottommost layer

of MoS_2 atoms were held fixed, and the topmost 0.3 nm of atoms of the tip were treated as rigid body. A Langevin thermostat was applied to the free atoms in the system to maintain the desired temperature (timestep of 1 fs). Simulations were performed in LAMMPS⁴⁴ package.

For further analysis, a previously published numerical solution to the 2D PTT model³⁵ was used to investigate the effect of different parameters on friction trends. This model uses a fourth-order Runge-Kutta approach to calculate the friction force and trajectory of an atom sliding across a 2D potential energy landscape. Simulations were run at scanning speeds of 100 nm/s, chosen to be within the experimental measurement range. Temperatures were varied from 5-350 K to capture the experimental temperature range. Lateral stiffnesses of 0.1, 1, and 10 N/m were compared, as the lateral stiffnesses of the experiments ranged over similar orders (the lateral force spring constants used in the experiments are reported in the Methods section; resulting total lateral stiffness values were obtained from the slopes of measured friction loops). The energy barrier was varied from 48-200 meV, a range on the order of the expected barrier for MoS₂.^{29,31,45} Scanning was performed along a path 40° from the zigzag axis of a 2D hexagonal lattice with a lattice parameter a=0.3 nm, similar to the 0.32 nm lattice constant of MoS₂. Twenty stick slip events were simulated for each scan, with the reported friction force being the average of five scans, with error bars representing the standard deviation of the friction force.

III. RESULTS AND DISCUSSION

A. Thermolubric behavior

Fig. 1 shows a set of friction vs. temperature vs. speed measurements for a silicon nitride tip.

There is a dramatic change in friction force as a function of temperature, and an observable

dependence on scanning speed as well. The general thermolubric effect predicted by the PTT model and by the MB model (at higher temperatures) occurs, 11,12,15–19,23,24,46 with a decrease in friction force of roughly 100x as temperature increases from 166 K to 466 K. An approximately logarithmic increase in friction force with scanning speed is also seen. The temperature dependence is consistent with the reports of Zhao et al., 29 except that here we do not see an athermal region below 220K, nor do we observe any wear as confirmed by imaging the scanned and surrounding surface both before and after testing. Atomic lattice stick-slip behavior was observed at all temperatures and speeds, but there was more noise apparent at lower temperatures due to the flow of LN₂; representative examples at 166 K and 466 K are shown in Fig. 1(c,d). While friction measurements at low temperatures had larger relative noise than those at room temperature, lattice periodicity was sometimes clearly present, and was consistently confirmed via fast Fourier transform analysis. We did not observe any correlation between sample preparation method or thickness and the bifurcation of nanoscale thermolubric behavior.

To compare with previous work that used the PTT model to analyze speed-dependent friction behavior, $^{13-16}$ we initially fit the friction force vs. scanning speed data at room temperature using the transcendental form of the PTT model (Equation 1). The three fit parameters in Equation 1 are F_c , β , and f_0 . The fit equation agrees well with the data (see Fig. S2) and yields parameters of F_c = 58 ± 4 nN, β =(114 ± 60)x10⁶ N^{3/2}/J, and f_0 = 8 ± 2 MHz and a coefficient of determination of R²=0.80, based solely on the speed dependent data at room temperature. Given the observed stick-slip spacing of 0.317 ± 0.04 nm, a purely sinusoidal potential would yield β_{sin} = $3\pi\sqrt{F_c}/(2\sqrt{2}a)$ =(80 ± 34)x10⁶ N^{3/2}/J, which is in agreement with the fitted value. However, both the fitted and calculated values have large uncertainties due to the scatter in the data, likely due

to vibrational noise in the experiments, and possibly due to atomic-scale changes in tip structure that may occur during the experiments.

We then perform fitting of the data across the entire temperature range. The values of F_c , β , and f_0 are still fit parameters, but their values are constrained globally such that they are the same for all temperature-speed data. In this way, the fit finds the parameters that best describe the dataset across all experimental temperatures and speeds with the PTT model. The results are shown in Fig. 2(a). While they do produce a fit that shows friction increasing with increasing speed and decreasing with increasing temperature, the overall agreement between the experimental data and the fit is much weaker than the fit at a given temperature.

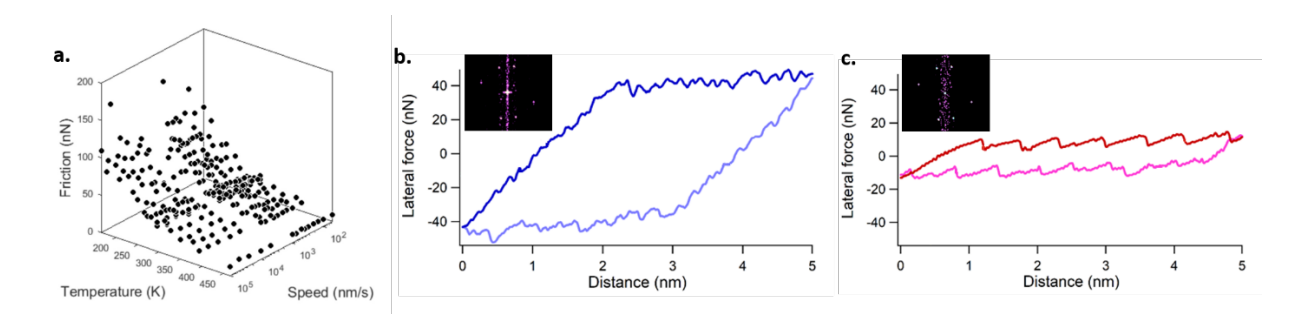


Figure 1: (a) The friction force between bulk MoS₂ and a silicon nitride tip varies strongly with temperature, and moderately with sliding speed. A rotatable version is available in the online supplementary material. (b,c) Friction loops and inset FFTs at 166 K and 466 K, respectively, taken at 16 nm/s and zero applied load. These experimental data are from dataset A in Table S-VII.

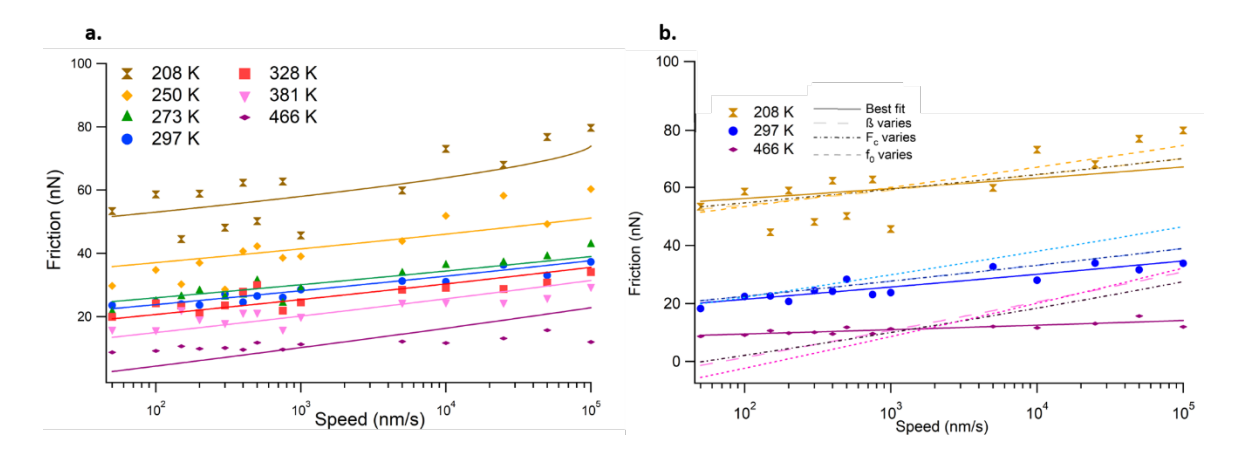


Figure 2: (a) Friction vs. speed experimental data (symbols) for a silicon nitride tip sliding against bulk MoS₂, with each color/symbol set measured at different temperatures. The graph shows a subset of the data in Fig. 1 for clarity, although the entire dataset was used for fitting to the PTT model (Equation 1 – lines). The resulting parameters extracted from the global fit of Equation 1 to the entire temperature-speed parameter set are $F_c = 142 \pm 5$ nN, $\beta = (50 \pm 3) \times 10^6$ N^{3/2}/J, and $f_0 = 600 \pm 100$ MHz. (b) Friction vs. speed experimental data (symbols) at three selected temperatures, fit with all parameters varying with temperature (solid lines), and also fit with each individual parameter varying with temperature (dashed lines). The fit is greatly improved when all parameters are allowed to vary with temperature, suggesting the PTT model is more appropriate for friction vs. speed behavior than friction vs. temperature. Parameters are given in Tables SI-V. The experimental data are from dataset A in Table S-VII.

As mentioned above, the only other previous study in which the PTT model was fit to friction vs. temperature and speed in vacuum conditions was the work of Jansen et al. for Si sliding on HOPG along a crystallographic direction chosen to minimize zig-zag motion²⁵. Similar to our results above, they found that the quality of the fit was not satisfactory when F_c , β , and f_0 were

treated as temperature-independent variables. Jansen et al²⁵ were able to improve the quality of the fit of the PTT model to their data by letting f_0 vary freely for each temperature, and found the best fit produced non-monotonic variation of f_0 with temperature. As Jansen *et al.* discuss, while temperature dependence of f_0 is indeed possible, a model for such dependence has not yet been proposed.

Regardless, in the same manner, we treated f_0 as a free parameter vs. temperature for the dataset in Fig. 1, while β and F_c were held constant. This produced slightly better fits, with R²=0.62, although the model still did not agree well with the dataset overall (see Fig. 2(b) and S3). The attempt frequency also varied with temperature by more than 6 orders of magnitude, from kHz to GHz, exhibiting an overall increasing trend with temperature but with noise and nonmonotonicity (see Fig. 3(a) and Table S-II). The dependence of f_0 on temperature did not fit any common functions we attempted (logarithmic, exponential, trigonometric, quadratic, power law functions). The best fit values of f_0 were either similar to or higher than those reported in previous work, albeit for different materials. 13,14,16 The value of f_0 affects the speed at which a plateau in the friction-speed dependence of the PTT model appears^{46,47}. For example, Riedo et al.¹⁶ observed a plateau at approximately 9 μm/s for Si sliding on mica, and Liu et al. 14 saw plateaus at 1-4 μm/s for a Si tip sliding on Au in UHV. Li et al. 13 did not see a plateau for a Pt tip sliding on Au in UHV, which they attribute to their experimental limitation of speeds being less than 1 μm/s. Since no plateau was resolved in our experiments, the values of f_0 from the fits cannot be compared to a measured value. As well, it has been proposed that the plateau can relate to mechanical noise in the system. 16,47 The lack of a plateau in this work may be related to specific mechanical properties of our AFM system, including at the fast scanning speeds used. Note that speed dependence without a plateau (where, at higher speeds, either a more rapid increase, or even a decrease in friction, is seen as a function of the natural logarithm of speed) has been predicted in other work, and was attributed to the changing role of dissipative and inertial mechanisms as a function of speed.^{48,49}

To further test the model, we performed similar global fits with β as the free parameter that varies with temperature (Fig. 3(b)). Similar to the variance in f_0 , β showed a non-monotonic trend with temperature (values given in Table S-IV), varying by a factor of 4.5 over our measured temperature range. To our knowledge, there is no physical motivation that has been proposed to cause β to vary in this manner. As β is related to the shape of the potential energy of the surface, no significant change over temperature is expected if the MoS2 does not undergo any structural phase transitions. The only structural change that could affect friction is thermal expansion corresponds to less than 100 parts per million strain over the temperature range we have studied. 50 While an effect of lattice spacing on friction has been seen in experiments and simulations, ¹⁰ the effect occurred for changes in lattice parameters that were over 500 times greater than that which thermal expansion would cause for our temperature range. We note that the energy corrugation predicted by the sinusoidal form with the best fit values of Fig. 2(a) is 3.3x10⁶ N^{3/2}/J. This falls within the range of our experimentally extracted values, despite the actual surface potential likely not being a perfect sinusoid. As with f_0 , the dependence of β on temperature did not fit any common functions we attempted (logarithmic, exponential, trigonometric, quadratic, power law functions).

There was a monotonic trend observed when F_c was the free parameter with temperature, as seen in Fig. 3(c). F_c increased approximately exponentially as temperature decreased (see Section S2), becoming twice as large at 140 K than at 500 K. In the PTT model, F_c is the static friction at 0 K and it depends only on the energy barrier and the lattice spacing, neither of which will change appreciably with temperature. This effect was not caused by tip changes either, as the temperature was ramped up and back down without any systematic change in friction force. While this parameter does phenomenologically change with temperature, there is no physical explanation consistent with the assumptions within the PTT model, further suggesting that there are limits to the scientific utility of the PTT model.

In any case, letting f_0 , F_c , or β vary individually with temperature does not produce a significantly improved fit of the PTT model to the data. As shown in Fig. 2(b), the fit of friction vs speed at a single temperature matches the experimental data with good accuracy. Any of the global fits show much less agreement, especially at high and low temperatures. Thus, the PTT model is a better tool to investigate frictional behavior as a function of speed than as a function of temperature.

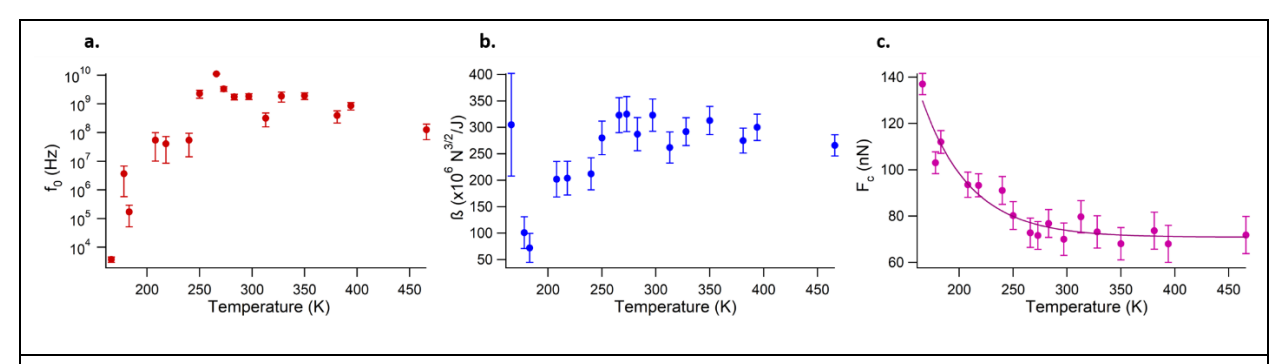


Figure 3: Fits of the PTT model to friction data for a silicon nitride tip sliding against bulk MoS₂; original data set shown in Figure 1 (from dataset A in Table S-VII). (a) f_0 , (b) β , and (c) F_c vs

temperature when each parameter was allowed to vary while fitting, respectively. F_c fits well to a negative exponential function (see Section S2), while f_0 and β vs. temperature do not fit well to any common functional form.

A better sense of the differences between experiment and the PTT model's thermal behavior was obtained by considering the friction force as a function of temperature. In multiple experiments, we observed strong thermolubricity across a range of speeds, such as in Fig. 1 and the example shown in Fig. 4(a). In these cases, friction forces at low temperatures were approximately two orders of magnitude higher than those above room temperature.

However, fitting the temperature-dependent data with the PTT model at a single sliding speed gave relatively poor agreement with the results in both the thermal activation and thermal drift regimes. Fig. 4(b), which is a subset of the dataset shown in Fig. 1 taken at the speed of $100 \, \mu m/s$, clearly shows that neither the predictions for the thermal activation regime (Equation 2) nor for the thermal drift regime (Equation 3) fit the observed behavior well: the thermal activation fit did not capture the dataset's convexity, and the thermal drift fit was too convex. The failures of the PTT model in either regime to fit the entire data set become more apparent when viewing 3D renderings of these two fits, which are shown in Fig. 5, with a rotatable version of these graphs available in the online supplementary material. The fit showed that the curvature and shape of the colored surfaces representing the PTT thermal activation and thermal drift models did not agree well with the experimental data, with R^2 values of 0.58 and -1.05, respectively. Another experimental dataset taken with a different tip, in this case a silicon tip presumed to have a silicon oxide termination, is shown in Fig. S4 for further comparison. Again, agreement with the PTT

model is poor, as quantified by the R^2 values of 0.19 and -1.2 for the thermal activation and thermal drift models respectively.

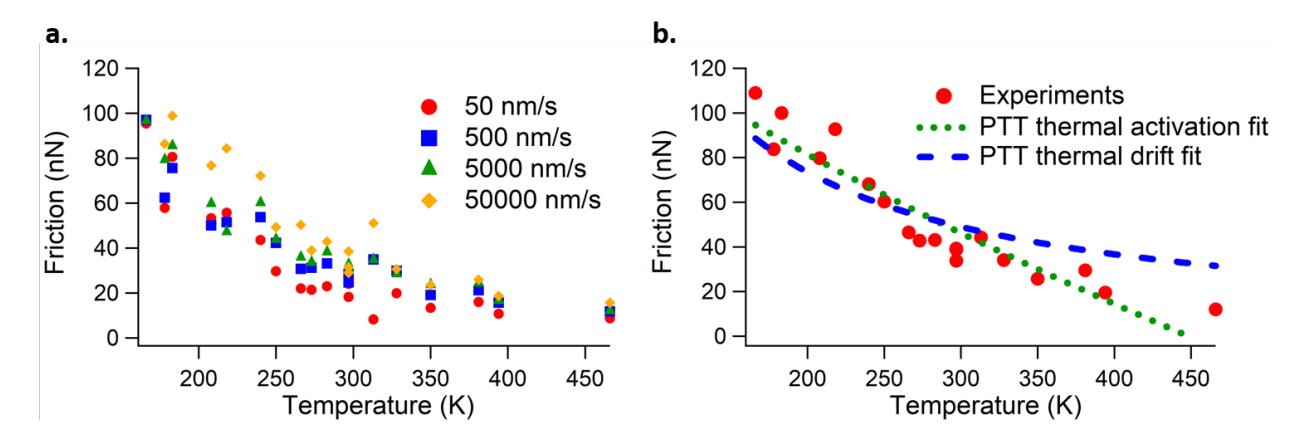


Figure 4: (a) The friction force vs temperature between bulk MoS₂ and a silicon nitride tip at multiple sliding speeds shows thermolubricity. These data are a subset of those in Fig. 1, with only four speeds shown for clarity. (b) The temperature dependent data (red circles) are another subset of the data shown in Fig. 1 that was taken at 100 μ m/s between bulk MoS₂ and a silicon nitride tip. It was fit to both the thermal activation (green dotted line) and thermal drift (blue dashes) equations. Neither produces convincing fits although the thermal activation fit is better. Fit parameters for the thermal activation (Equation 2) were F_c =190 ± 90 nN, β =(6.1 ± 0.2)x10⁶ N^{3/2}/J, and f_0 =(5 ± 0.2)x10¹² Hz. Fit parameters for the thermal drift regime (Equation 3) were U=0.016 ± 0.005 meV and the combined value for $C*\eta m$ =(8 ± 2)x10⁵ (the variables cannot be decisively separated). The data are from dataset A in Table S-VII.

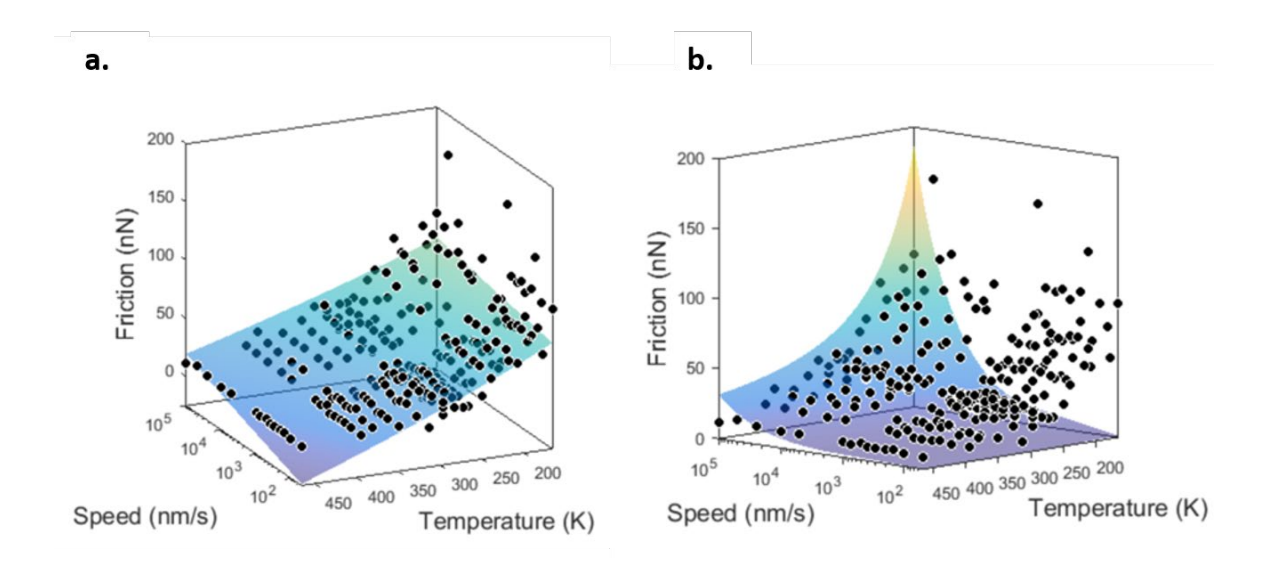


Figure 5: The (a) thermal activation and (b) thermal drift regimes of the PTT model are used to fit experimental data shown in Fig. 1-4. The fit is poor, as quantified by R² values of 0.58 and -1.05, respectively. The experimental data are from dataset A in Table S-VII.

To better understand the universality of the temperature-dependent behavior, we ran complementary MD simulations using a silicon nitride tip and a MoS₂ countersurface. While the MD simulations did not explore the speed dependence of friction comprehensively (only two speeds were tested, both of which are far greater than AFM experimental speeds due to the limitations of standard MD algorithms), they provided a test system independent of experimental complications such as mechanical noise. The MD simulations also produce a strong decrease of friction with temperature, although not as strong as the experiments. In particular, friction decreased by a factor of approximately 3 as the temperature was increased from 208 to 466 K. Note that, while the tip size and load were matched to that of the experiments in Fig. 1, the friction force values and change in friction force are much smaller. This difference is likely due to the difference in lateral stiffness between MD and AFM, which could not be optimally matched

due to the computational expense of using a very compliant spring. When compared to the PTT model, the fit is poor as well, as seen in Fig. 7, with R^2 values of 0.82 and -0.86 (again, a rotatable version is available in the online supplementary material).

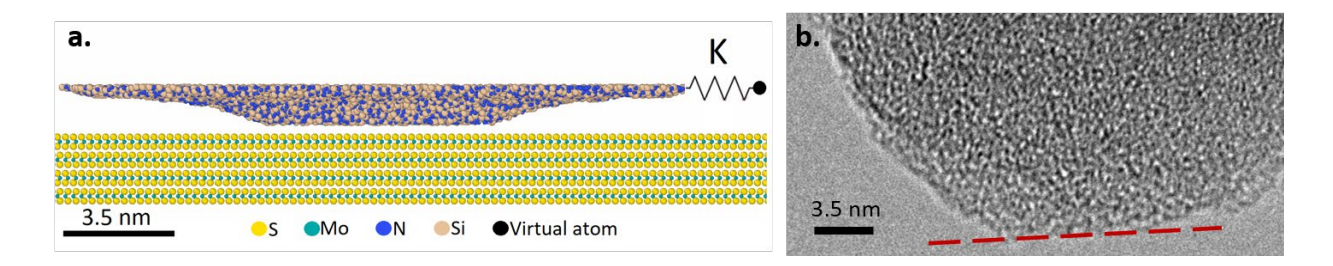


Figure 6: (a) MD model developed consist of an amorphous Si_3N_4 tip slid over a MoS_2 substrate using a spring and a virtual atom representing cantilever. (b) TEM image of one of the AFM tips used (this particular tip was used to collect the data shown in Fig. 1). The dashed red line indicates the orientation of the sample and the resulting region of contact.

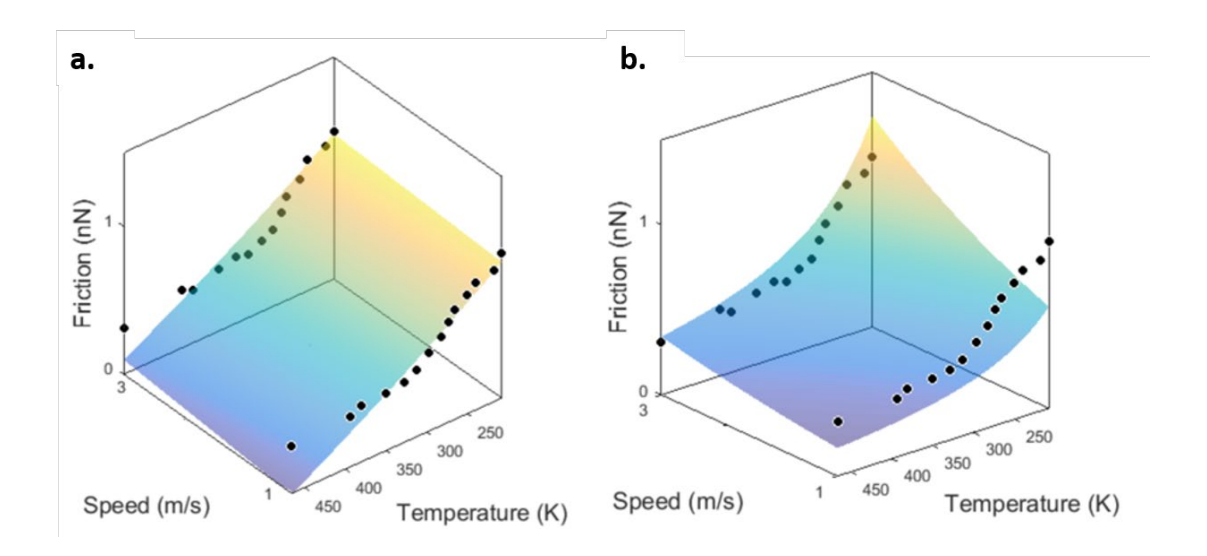


Figure 7: Results from MD simulations (black circles). The fits to the (a) thermal activation and (b) thermal drift regimes (colored surfaces) also do not fit particularly well to the simulated data, with an R² of 0.82 and -0.86, respectively.

This disagreement with predictive models extends beyond the basic formulation of the PTT model. Data were compared with other models by Müser et al.⁵¹, Krylov et al.⁵², Perez et al.³², Jahangi et al.⁵³, and Reimann et al.⁴⁸, with poor agreement seen for all, quantified by an R² value of <0.5. Model equations and R² values are given in Table S-VII.

Attempts to find an analytical equation that represented the thermolubric behavior across the speed range led to the development of a phenomenological fit equation of

$$F_f = A \exp(E_0/k_B T) \ln(Bv/T), \tag{4}$$

where E_0 is an energy barrier, k_B is the Boltzmann constant, v is the scanning speed, T is the temperature, and A and B are fit parameters with units of N and K•s/m. The fit is substantially better than all other forms investigated, with R^2 values of 0.89, 0.92, and 0.80 for the first experimental data set (see Fig. 8(a) for the fit of Equation 4 to that dataset), the second experimental data set shown in Fig. S4 (see Fig. S4(c) for the fit of Equation 4 to that dataset) and the MD simulation data (see Fig. 8(b) for the fit of Equation 4 to that dataset). The associated fit parameters are given in Table S-VI. This equation is informed by the often-seen logarithmic dependence of friction force on scanning speed and an exponential energy barrier term, although there is no physical underpinning to support why the logarithmic speed dependence and exponential energy barrier terms should appear as a product.

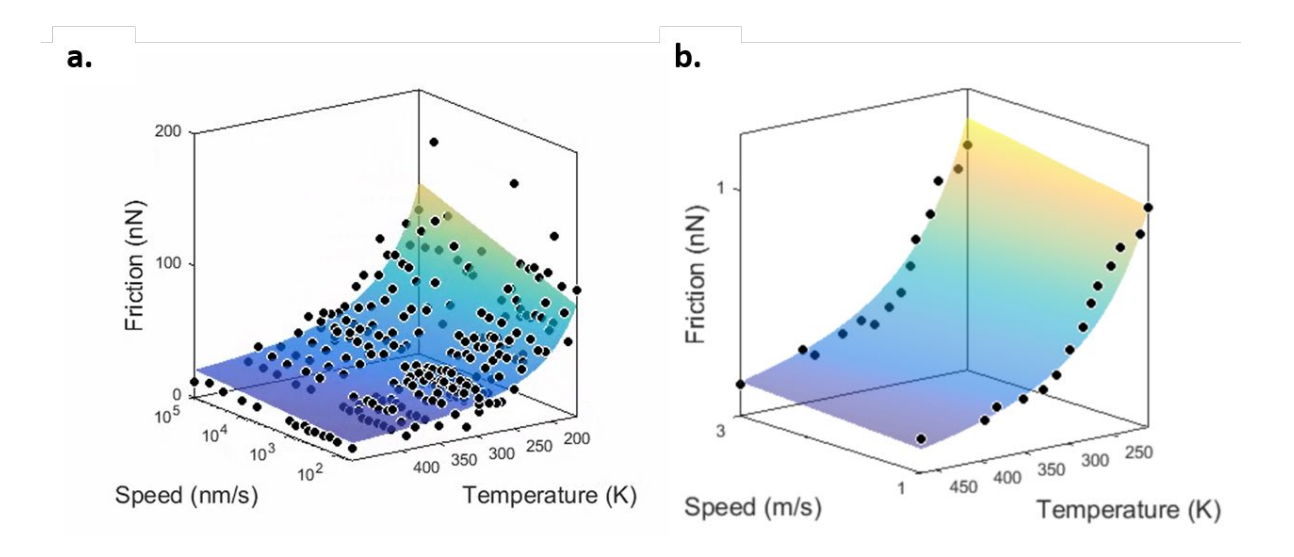


Figure 8: The phenomenological model (Equation 4) presented in this work provides a much better fit to the (a) experimental results (shown in Fig. 1-4) and (b) simulation results (shown in Fig. 7). The fit is quantified with R² values of 0.89 and 0.92, respectively. The data in (a) are from dataset D in Table S-VII.

B. Athermal behavior

As mentioned above, a strong thermolubric dependence of friction force for AFM tips sliding on MoS₂ is clearly seen in Fig. 1 and in multiple replicate experiments with other tips, including silicon and silicon nitride tips. However, the strong drop of friction with temperature is not always observed. Fig. 9 shows data obtained under nominally identical conditions, but no discernable temperature dependence is seen, and friction is low at all temperatures. Both types of behavior are seen in multiple independent data sets, with four datasets showing thermolubricity and six datasets showing athermal, low friction behavior. The behavior is essentially bifurcated. When thermolubricity is seen, a friction force increase of 4-20 times is observed as temperature decreases (reaching values of the order of 10-100 nN at the lowest temperature of 150 K). The

highest friction force is at least two standard deviations above the median value. In contrast, in the athermal cases, the mean friction forces are significantly lower, on the order of single nN, and the range of friction values is much lower, with almost all values within a standard deviation of the median Although the absolute value of the friction force will vary with tip size as well as tip material, tip atomic structure, and tip surface energy, there is a clear split in friction force magnitude between the thermal and athermal cases, with the athermal cases being significantly lower. A summary of the experiments conducted is provided in Table S-VII. Such strongly differing nanoscale friction behavior for the same nominal system has not been previously reported in the literature.

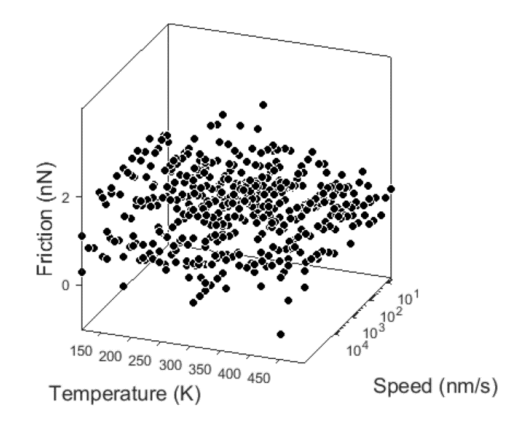


Figure 9: Friction force vs. speed and temperature for a Si tip sliding on monolayer MoS_2 . This is a representative example from the six (F_f, v, T) datasets where no discernable trend with temperature and sliding speed is seen. A

rotatable version is available in the online supplementary material.

We now consider a possible explanation for this strong contrast in behavior. The thermolubricity predicted by the PTT model is attributed to the thermal energy approaching the magnitude of the energy barrier to sliding as the temperature increases. However, if the energy barrier to sliding is sufficiently low, there will be minimal thermal effects and friction will be low. This suggests that the athermal cases occur when the energy barrier to sliding was on the order of k_BT for T=150 K at most, which corresponds to an energy of 12.9 meV. Reasons for a change in energy barrier will be discussed further below, but first we examine more carefully the relationship between the energy barrier, the temperature dependence of friction, and the overall magnitude of friction forces.

Using the 2D PTT numerical model,³⁵ the friction force and sliding pathway can be determined for a given set of values for the scanning speed, temperature, lateral stiffness, and energy barrier. Results from this numerical model in Fig. 10 clearly show that, as expected, as the energy barrier decreases, friction reduces, and exhibits no clear trend with temperature above 150 K for an energy barrier of 100 meV or less. An increase in friction is only observed at much lower temperatures; this is consistent with work by Steiner et al. using a similar 2D numerical model.³³ If the athermal experimental data are fit with the equation for the thermal drift regime of the PTT model (Equation 3), the best fit surface is a nearly horizontal plane intersecting the experimental data. However, the lack of any distinctive features such as an upturn at low

temperatures or a plateau at high speeds, combined with the number of fit parameters, severely limit the ability to reliably extract parameters from such a fit. Even for an energy barrier as high as 200 meV, the greatest variation in frictional behavior obtained by the 2D PTT numerical model is seen at temperatures below 100 K (Fig. 10). The liquid nitrogen cooling system used in the experiments reaches an absolute minimum sample temperature of 120 K, meaning that some of the strongest variation may be in an experimentally inaccessible regime.

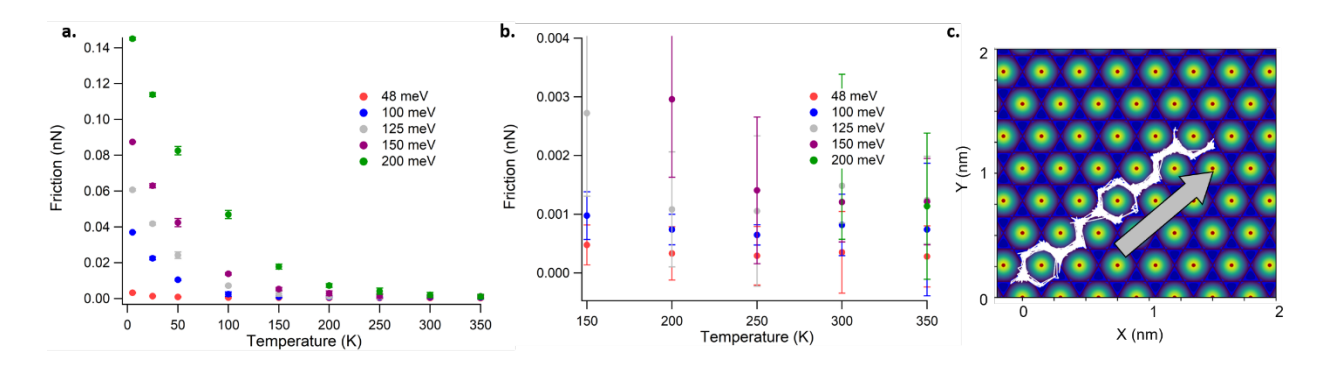


Figure 10: The 2D PTT numerical model was used to calculate friction force vs temperature for a range of energy barriers. (a) There is a clear decrease in friction force with increasing temperature for energy barriers above 100 meV, and a small decrease at lower energy barriers. (b) Restricting the temperature to the experimentally achievable range of >150 K demonstrates that friction forces in cases with low energy barriers (plotted here for barriers of 100 meV or less) show a large scatter and little temperature dependence. The error bars represent the standard deviation from five calculations for each condition. Friction forces above 0.004 nN (obtained at low temperatures for the two largest energy barriers) are outside of the plotted range. (c) The simulated pathway of the tip from the 2D PTT model algorithm is shown in white. The white region is a dense array of points representing the position of the tip at each timestep in the

simulation. There are many small deviations around atoms in directions other than the direction of pulling (indicated by the arrow), including some that backtrack along the previous path. This plot was acquired with the parameters E_0 =200 meV, k=1 N/m, and T=300 K.

The barrier for a tip-sample contact has been shown to be on the order of 100s of meV for a nanoscale tip sliding on MoS₂.^{29,45} If the energy barrier is on the same order as the thermal energy, the key assumption of the PTT model for the activated regime (and for several related models) that transitions are infrequent is not valid. Moreover, there would be a strong chance of backward jumps, which are ignored in the thermal activation regime of the PTT model. Thus, the strong decrease in friction across all temperatures as the energy barrier is decreased according to the 2D PTT model (Fig. 10) is not surprising. In addition, the unavoidable mechanical noise in any experimental system can also provide energy that further assists in overcoming the energy barrier to sliding.^{47,54}

The 2D PTT numerical model allows for deviations of the path of the point mass from the direction of pulling, an effect that the 1D PTT model obviously cannot capture. Those deviations from the pulling direction can be orthogonal to the direction of motion, but in the PTT simulations conduced, for some cases the tip moved backwards, violating the assumption of no backwards jumps in the traditional PTT model in the activated regime. Fig. 10(c) and the corresponding video available in the online supplementary material shows a pathway from the PPT model for an energy barrier of 200 meV with sliding at room temperature, which demonstrates this behavior.

The lateral system stiffness (determined in practice by the lateral stiffness of the AFM cantilever spring, the contact,⁵⁵ and the tip structure⁵⁶) also affects the frictional force and its temperature dependence, with a smaller lateral stiffness leading to higher friction (see Fig. S5). At room temperature, the difference is not pronounced. However, at low temperatures, a lower stiffness leads to an increase in friction. In particular, for an energy barrier of 200 meV, thermolubric behavior is seen for low lateral stiffness values (k=0.1 or 1 N/m), while athermal behavior at low friction is seen for high lateral stiffness values (10 N/m). This occurs because a more elastic compliance will permit larger lateral elastic deformations (be it in the cantilever spring, the tip structure itself, or in the contact) before the slip instability occurs, enabling the tip to slip single or multiple lattice sites when the critical slip condition is approached. This is explicitly seen in some of the 2D PTT numerical model friction traces, in that the initial stick portion is significantly larger at low temperatures (see Fig. S6). In experiments, this change in stiffness can result from interface changes such as contamination or small atomic rearrangements at the end of the tip as well as the cantilever. The onset and magnitude of this effect depends on the energy barrier, since the competition between barrier height, spring stiffness, and thermal energy drives slip instabilities.

Based on these results, we propose that either differences in the effective energy barrier and/or the total lateral stiffness from one set of experiments to the next cause the change from thermolubric to athermal behavior. A change in energy barrier could arise from multiple factors. One such factor is the tip shape, size, and atomic structure. A larger and/or flatter tip will lead to larger contact areas for otherwise the same experimental conditions (e.g. applied load, scanning speed, temperature, materials). Changing the number of atoms interacting at the interface can

alter the barrier to sliding. Recently, Gao et al. modeled the effect of contact size dependence on atomic friction by considering the scale-dependent shear stress that occurs for Peierls-type dislocation-mediated interfacial slip between elastic solids.⁵⁷ This is an improvement over the PTT model since elastic deformation and variability in the contact size are explicitly included. In this model, small contact sizes exhibit relative high barriers to slip (high shear strengths) since slip must occur homogeneously (i.e. concurrent slip of all atoms at once that requires attaining a stress, just as the yield strength of a defect-free crystal approaches a high, ideal value). At larger contact sizes, more facile dislocation nucleation and propagation lead to a decrease in energy barrier and shear strength.⁵⁸

Such a dislocation-focused model is appropriate for ordered interfaces; here, the tip is amorphous and additional study is required to describe such an interface. However, the model does consider the effect of interfacial incommensurability and shows that friction is greatly reduced by incommensurability, as observed in experiments, ⁵⁹ but still finite, since elastic deformations can enhance the interfacial energy at preferred positions. In our experiments, the atomic structure of the end of the tip can certainly vary. Tips made of SiN_x or Si with its native oxide will be amorphous, while UNCD tips are polycrystalline and may have defects including grain boundaries and disordered carbon at the end of the tip.⁶⁰ The degree of commensurability may thus have varied substantially between the different tips used in this experiment. As well, while the tip structure may also change during the experiment, by excluding data sets where adhesion forces varied widely, we propose that the data presented here represents measurements for at least moderately stable tip sizes and structures. A tip structure that leads to an incommensurate tip-sample contact will have a low barrier to sliding, and thus may be

expected to exhibit low, athermal friction behavior. Robbins and co-workers have shown using atomistic simulations that the contact stiffness can change significantly (even orders of magnitude) depending on the nature of atomic alignment at the interface, as determined by the degree of crystallinity of each surface, and of atomic-scale roughness.^{61,62}

Surface cleanliness can also affect the strength of the tip/sample interaction, as has been reported previously. 63-65 While the UHV environment (< 8x10-10 Torr) of the experiments is indeed very clean, some amount of contamination still remains. Quadrupole mass spectrometry analysis of this UHV chamber reveals trace amounts of H₂, N₂, CO, CO₂, CH₄, and various larger hydrocarbons. Most of these species have very low adsorption and desorption energies on MoS₂, except for the hydrocarbons. While the coverage of these species will likely be sparse, the surface coverage can increase as temperature decreases, particularly for the larger hydrocarbons. 66,67 During a representative test, chamber pressure was seen to decrease from 10⁻⁹ Torr to 7x10⁻¹⁰ Torr as the sample temperature decreased from 300 K to 150 K. While the sample will be at somewhat higher than the LN₂ connection lines, it will still be significantly lower than the rest of the chamber and the AFM scanning head. Earlier work in the literature shows that interfacial adsorbates can provide pining sites at incommensurate interfaces, leading to a significant increase in the friction force. 63 Similarly, in recent MD simulations, Ouyang et al. observed an initial increase in friction force between tip and sample with increasing adsorbate coverage, followed by a decrease as surface coverage further increased. 65 For weakly bound adsorbates and at low temperatures, which are the conditions relevant to the present experiments, Ouyang et al. observed that the tip displaces adsorbates along the surface when sliding, thus creating an additional mode of frictional dissipation and increasing the energy barrier to slip. As another

example of the strong effect of adsorbates on friction, work investigating the friction force required to laterally displace antimony islands on graphite by AFM tips saw bifurcated behavior, with a fraction of the islands exhibiting very low friction, and others exhibiting a strong increase in friction force with increasing contact area. The behavior was attributed to adsorbates between the nanoparticle and countersurface, pinning the incommensurate interface.⁶⁸

While obvious areas of contamination were avoided in the experiments, adsorbates on the tip are not observable, along with adsorbates that have been pushed to the edges of the scan area. Thus, the presence of adsorbates is possible. To test the hypothesis that varying amounts of adsorbates for the bifurcated temperature dependence, we increased the chamber pressure from its initial value of 1x10⁻⁹ Torr by throttling the ion pump attached to the UHV system. We did observe a roughly twofold increase in friction initially. However, friction then plateaued as the pressure was further increased. Near the highest pressure tested (7.3x10⁻⁸ Torr), friction decreased tenfold and then increased again, showing substantial variation at the same nominal pressure (see Fig. S7). Upon reducing the pressure, friction recovered to nearly the same value seen previously. These changes with pressure suggest that adsorbates may play a role in the bifurcated behavior we have observed (see SI). We do not claim that adsorbates are the cause of the thermal or athermal behavior, only that they can have effects not always considered in UHV experiments. Further work is needed to determine their potential role. Patchy or heterogeneous adsorbate coverages could also create or enhance the discrepancy between the thermal and athermal behavior reported here. This will be the subject of future study.

IV. CONCLUSIONS

In conclusion, we have observed strong thermolubricity of nanoscale friction on MoS_2 over a wide range of sliding speeds, with a friction decrease of up to 100x in experiments at $100 \,\mu\text{m/s}$ and 3x in simulations at 1 m/s across temperatures from 208-466 K. This thermolubricity is not always present, with athermal, low friction seen just as often. We attribute this behavior to fluctuations of the energy barrier of the tip-sample potential energy surface, possibly due to changes in tip structure and/or the presence of adsorbates.

The thermolubric results are fit to the PTT model and other established models; none are able to capture the temperature dependence convincingly. Work with numerical simulations using a 2D PTT model suggest that the energy barrier and the lateral stiffness, both of which can be affected by the precise nature of the tip-sample interfacial interaction, are crucial factors for the temperature trends. The assumptions of a high energy barrier and no backwards hopping in the traditional PTT model may not be reasonable in many situations, such as for the 2D and layered materials traditionally found to have low friction.

This work shows that temperature dependence of nanoscale friction does not necessarily have a straightforward interpretation. Friction is dependent not only on the system temperature but on the atomic-scale details of the structure at the tip-sample interface, which can change due to contamination and tip geometry, among other factors. The idea that thermal energy lowers static friction as temperature increases is valid, but the physical underpinnings of the PTT model involve assumptions that leave out important pieces of information needed to render it consistent with experiments.

ACKNOWLEDGMENTS

This work was funded by the National Science Foundation, awards CMMI-1762384 and CMMI-1761874. Simulations were run using the Extreme Science and Engineering Discovery Environment (XSEDE), which was supported by National Science Foundation (NSF) Grant No. ACI-1548562. We gratefully acknowledge Dr. Mengqiang Zhao of the A.T. Johnson group at University of Pennsylvania, who grew the monolayer MoS₂ samples used in this work.

¹ T.W. Scharf and S. V. Prasad, J. Mater. Sci. **48**, 511 (2013).

² P. Kumar and M.F. Wani, **2004**, (2018).

³ N. Rajendhran, S. Palanisamy, P. Periyasamy, and R. Venkatachalam, Tribol. Int. **118**, 314 (2018).

⁴ H. Xiao and S. Liu, Mater. Des. **135**, 319 (2017).

⁵ K. Tripathi, G. Gyawali, and S.W. Lee, ACS Appl. Mater. Interfaces **9**, 32336 (2017).

⁶ H. Xu, J. Zang, Y. Yuan, P. Tian, and Y. Wang, Appl. Surf. Sci. **492**, 199 (2019).

⁷ J.C. Burton, P. Taborek, and J.E. Rutledge, Tribol. Lett. **23**, 131 (2006).

⁸ C.G. Dunckle, M. Aggleton, J. Glassman, and P. Taborek, Tribol. Int. 44, 1819 (2011).

⁹ M. a. Hamilton, L. a. Alvarez, N. a. Mauntler, N. Argibay, R. Colbert, D.L. Burris, C. Muratore, A. a. Voevodin, S.S. Perry, and W.G. Sawyer, Tribol. Lett. **32**, 91 (2008).

¹⁰ M.R. Vazirisereshk, K. Hasz, M.-Q. Zhao, A.T.C. Johnson, R.W. Carpick, and A. Martini, ACS

Nano (2020).

- ¹¹ A. Schirmeisen, L. Jansen, H. Hölscher, and H. Fuchs, Appl. Phys. Lett. **88**, 21 (2006).
- ¹² I. Barel, M. Urbakh, L. Jansen, and A. Schirmeisen, Tribol. Lett. **39**, 311 (2010).
- ¹³ Q. Li, Y. Dong, D. Perez, A. Martini, and R.W. Carpick, Phys. Rev. Lett. **106**, 126101 (2011).
- ¹⁴ Z. Ye, Y. Dong, P. Egberts, R.W. Carpick, A. Martini, X.-Z.Z. Liu, Z. Ye, Y. Dong, P. Egberts, R.W. Carpick, and A. Martini, Phys. Rev. Lett. **114**, 1 (2015).
- ¹⁵ Y. Sang, M. Dubé, M. Grant, M. Dube, and M. Grant, Phys. R **87**, 1 (2001).
- ¹⁶ E. Riedo, E. Gnecco, R. Bennewitz, E. Meyer, and H. Brune, Phys. Rev. Lett. **91**, 084502 (2003).
- ¹⁷ V.L. Popov and J. a T. Gray, ZAMM Zeitschrift Fur Angew. Math. Und Mech. **92**, 683 (2012).
- ¹⁸ G.A. Tomlinson, CVI. A Molecular Theory of Friction (1929).
- ¹⁹ L. Prandtl, Zeitschrift Für Angew. **8**, 85 (1928).
- ²⁰ S.Y. Krylov, K.B. Jinesh, H. Valk, M. Dienwiebel, and J.W.M. Frenken, Phys. Rev. E Stat. Nonlinear, Soft Matter Phys. **71**, 1 (2005).
- ²¹ M.Z. Baykara, M.R. Vazirisereshk, and A. Martini, Appl. Phys. Rev. **5**, (2018).
- ²² K.B. Jinesh, S.Y. Krylov, H. Valk, M. Dienwiebel, and J.W.M. Frenken, Phys. Rev. B Condens. Matter Mater. Phys. **78**, 1 (2008).
- ²³ I. Barel, M. Urbakh, L. Jansen, and a. Schirmeisen, Phys. Rev. B Condens. Matter Mater. Phys. **84**, 1 (2011).
- ²⁴ I. Barel, M. Urbakh, L. Jansen, and A. Schirmeisen, Phys. Rev. Lett. **104**, 1 (2010).
- ²⁵ L. Jansen, H. Hölscher, H. Fuchs, and A. Schirmeisen, Phys. Rev. Lett. **104**, 256101 (2010).
- ²⁶ O. Acikgoz and M.Z. Baykara, Appl. Phys. Lett. **071603**, (2020).
- ²⁷ B.C. Tran-Khac, H.J. Kim, F.W. DelRio, and K.H. Chung, Appl. Surf. Sci. **483**, 34 (2019).

- ²⁸ X. Zhao, M. Hamilton, W.G. Sawyer, and S.S. Perry, Tribol. Lett. **27**, 113 (2007).
- ²⁹ X. Zhao, S.R. Phillpot, W.G. Sawyer, S.B. Sinnott, and S.S. Perry, Phys. Rev. Lett. **102**, 186102 (2009).
- ³⁰ X. Zhao and S.S. Perry, Tribol. Lett. **39**, 169 (2010).
- ³¹ Y. Liu, K. Wang, Q. Xu, and J. Zhang, (2020).
- ³² D. Perez, Y. Dong, A. Martini, and A.F. Voter, Phys. Rev. B Condens. Matter Mater. Phys. **81**, 1 (2010).
- ³³ P. Steiner, R. Roth, E. Gnecco, A. Baratoff, S. Maier, T. Glatzel, and E. Meyer, Phys. Rev. B Condens. Matter Mater. Phys. **79**, 1 (2009).
- ³⁴ S. Sills and R.M. Overney, Phys. Rev. Lett. **91**, 2000 (2003).
- ³⁵ Y. Dong, A. Vadakkepatt, and A. Martini, Tribol. Lett. **44**, 367 (2011).
- ³⁶ C.H. Naylor, N.J. Kybert, C. Schneier, J. Xi, G. Romero, J.G. Saven, R. Liu, and A.T.C. Johnson, ACS Nano **10**, 6173 (2016).
- ³⁷ H.-J. Butt and M. Jaschke, Nanotechnology **6**, 1 (1999).
- ³⁸ Q. Li, K.S. Kim, and a. Rydberg, Rev. Sci. Instrum. **77**, 1 (2006).
- ³⁹ T.D.B. Jacobs and R.W. Carpick, Nat. Nanotechnol. **8**, 108 (2013).
- ⁴⁰ S.B. Vishnubhotla, R. Chen, S.R. Khanal, X. Hu, A. Martini, and T.D.B. Jacobs, Tribol. Lett. **67**, 1 (2019).
- ⁴¹ J. Liu, J.K. Notbohm, R.W. Carpick, and K.T. Turner, ACS Nano **4**, 3763 (2010).
- ⁴² T. Liang, S.R. Phillpot, and S.B. Sinnott, Phys. Rev. B Condens. Matter Mater. Phys. **79**, 1 (2009).
- ⁴³ K. Matsunaga and Y. Iwamoto, J. Am. Ceram. Soc. **84**, 2213 (2001).

- ⁴⁴ S. Plimpton, J. Comput. Phys. **117**, 1 (1995).
- ⁴⁵ M.R. Vazirisereshk, K. Hasz, R.W. Carpick, and A. Martini, J. Phys. Chem. Lett. (2020).
- ⁴⁶ Y. Dong, D. Perez, H. Gao, A. Martini, Y. Dong, D. Perez, H. Gao, and A. Martini, J. Phys. Condens. Matter **24**, 265001 (2012).
- ⁴⁷ Y. Dong, H. Gao, A. Martini, and P. Egberts, Phys. Rev. E Stat. Nonlinear, Soft Matter Phys. **90**, 1 (2014).
- ⁴⁸ P. Reimann and M. Evstigneev, Phys. Rev. Lett. **93**, 230802 (2004).
- ⁴⁹ M. Evstigneev and P. Reimann, Phys. Rev. X **3**, 041020 (2013).
- ⁵⁰ Z. Lin, W. Liu, S. Tian, K. Zhu, Y. Huang, and Y. Yang, Sci. Rep. **11**, 1 (2021).
- ⁵¹ M.H. Müser, Phys. Rev. B Condens. Matter Mater. Phys. **84**, (2011).
- ⁵² S.Y. Krylov and J.W.M. Frenken, J. Phys. Condens. Matter **20**, 354003 (2008).
- ⁵³ S. Jahangiri, G.S. Heverly-coulson, and N.J. Mosey, **075406**, 1 (2016).
- ⁵⁴ S.Y. Krylov, J.W.M. Frenken, S.Y. Krylov, and J.W.M. Frenken, (2012).
- ⁵⁵ R.W. Carpick, D.F. Ogletree, and M. Salmeron, Appl. Phys. Lett. **70**, 1548 (1997).
- ⁵⁶ M. a Lantz and S.J. O'Shea, Appl. Phys. Lett. **70**, 970 (1997).
- ⁵⁷ Y. Gao, J. Mech. Phys. Solids **58**, 2023 (2010).
- ⁵⁸ Y. Dong, Q. Li, J. Wu, and A. Martini, Model. Simul. Mater. Sci. Eng. **19**, (2011).
- ⁵⁹ M. Dienwiebel, G.S. Verhoeven, N. Pradeep, J.W.M. Frenken, J.A. Heimberg, and H.W. Zandbergen, Phys. Rev. Lett. **92**, 126101 (2004).
- ⁶⁰ A. V. Sumant, D.S. Grierson, J.E. Gerbi, J. Birrell, U.D. Lanke, O. Auciello, J.A. Carlisle, and R.W. Carpick, Adv. Mater. **17**, 1039 (2005).
- ⁶¹ S. Akarapu, T. Sharp, and M.O. Robbins, Phys. Rev. Lett. **106**, 1 (2011).

- ⁶² B. Luan and M.O. Robbins, Phys. Rev. E Stat. Nonlinear, Soft Matter Phys. **74**, 1 (2006).
- ⁶³ G. He, M.H. Müser, and M.O. Robbins, Science (80-.). **284**, 1650 (1999).
- ⁶⁴ K. Hasz, Z. Ye, A. Martini, and R.W. Carpick, Phys. Rev. Mater. **2**, 1 (2018).
- ⁶⁵ W. Ouyang, A.S. De Wijn, and M. Urbakh, Nanoscale **10**, 6375 (2018).
- ⁶⁶ J.H. Thomas III and S.P. Sharma, J. Vac. Sci. Technol. **13**, 549 (1976).
- ⁶⁷ J.F. Weaver, A.F. Carlsson, and R.J. Madix, Surf. Sci. Rep. **50**, 107 (2003).
- ⁶⁸ D. Dietzel, C. Ritter, T. Mönninghoff, H. Fuchs, A. Schirmeisen, and U.D. Schwarz, Phys. Rev. Lett. **101**, 1 (2008).